Evolution of low-lying M1 modes in germanium isotopes

S. Frauendorf[1,*] and R. Schwengner[2]

[1]*Department of Physics, University of Notre Dame, Notre Dame, Indiana 46556, USA*
[2]*Helmholtz-Zentrum Dresden-Rossendorf, 01328 Dresden, Germany*

Magnetic dipole strength functions are determined for the series of germanium isotopes from $N = Z = 32$ to $N = 48$ on the basis of a large number of transition strengths calculated within the shell model. The evolution of the strength with increasing neutron number in the $1g_{9/2}$ orbital is analyzed. A bimodal structure comprising an enhancement toward low transition energy and a resonance in the region of the scissors mode is identified. The low-energy enhancement is strongest near closed shells, in particular at the almost completely filled $1g_{9/2}$ orbital, while the scissorslike resonance is most pronounced in the middle of the open shell, which correlates with the magnitude of the also deduced electric quadrupole transition strengths. The results are consistent with previous findings for the shorter series of iron isotopes and prove the occurrence and correlation of the two low-lying magnetic dipole modes as a global structural feature.

I. INTRODUCTION

The excitation and deexcitation of the nucleus by electromagnetic radiation at high excitation energy and high level density are described by means of γ-ray strength functions (γ-SF) which represent average transition strengths in a certain energy range. The experimental determination and the theoretical understanding of the properties of γ-SF have attracted increasing interest because of their importance for the accurate description of photonuclear reactions and the inverse radiative-capture reactions, which play a central role in the synthesis of the elements in various stellar environments [1,2]. The region of low transition energies is important for these processes. Traditionally, the γ-SF has been associated with electric dipole ($E1$) transitions. Recently a strong component of $M1$ character has been observed as an upbend of the γ-SF toward transition energy $E_\gamma = 0$.

First observed in ^{56,57}Fe [3], the upbend was found also in various nuclides in other mass regions, such as in Mo isotopes [4], in ^{105,106}Cd [5], and in Sm isotopes [6,7]. The experiments used light-ion induced reactions such as (^{3}He, ^{3}He'), and the data were analyzed with the so-called Oslo method to extract level densities and γ-SFs. This method was also applied in connection with β decay to ^{76}Ga [8]. A dominant dipole character of the low-energy strength was demonstrated in Ref. [9], and an indication for a magnetic dipole ($M1$) character was discussed for the case of ^{60}Ni [10].

Shell-model calculations revealed that a large number of $M1$ transitions between excited states produces an exponential increase of the γ-ray strength function that peaks at $E_\gamma \approx 0$ and describes the low-energy enhancement of dipole strength observed in Mo isotopes around the neutron shell closure at

$N = 50$ [11]. In these calculations, large reduced transition strengths $B(M1)$ appear for transitions linking states with configurations dominated by both protons and neutrons in high-j orbitals, the spins of which recouple. The low-energy enhancement was confirmed in shell-model calculations for ^{56,57}Fe [12], ^{46,50,54}Ti [13], and ^{44}Sc [14]. In the latter work, also the electric dipole ($E1$) strength function was calculated, which does not show an upbend comparable to that of the $M1$ strength. A correlation between the low-energy $M1$ strength [low-energy magnetic radiation (LEMAR)] and the scissors resonance (SR), a fundamental $M1$ excitation occurring in deformed nuclei around 3 MeV [15], was found in shell-model calculations for the series of isotopes from ^{60}Fe to ^{68}Fe [16]. It was found that the low-energy $M1$ strength decreases and the scissors strength develops when going into the open shell. The simultaneous appearance of the two $M1$ modes is in accordance with experimental findings in Sm isotopes [6,7]. Later on, $M1$ strength functions were calculated for isotopic series in various mass regions [17–19]. The study in Ref. [19] confirmed that the low-energy $M1$ strength is strongest in nuclides near shell closures.

In the present paper we study the low-energy γ-SFs for the chain of the Ge isotopes. The relatively small configuration space allows us to carry out shell-model calculations covering completely the open neutron shell $32 \leqslant N \leqslant 48$. We demonstrate for the first time that the low-energy $M1$ strength is concentrated in the LEMAR spike at the bottom of the shell, is partially moved into the SR in the middle of the shell, and is again concentrated in the LEMAR spike at the top of the shell.

II. SHELL-MODEL CALCULATIONS

The shell-model calculations for the germanium isotopes were carried out in the jj44pn model space with the jj44bpn

*sfrauend@nd.edu

Hamiltonian [20–22] using the code NUSHELLX@MSU [23]. The model space included the proton and neutron orbitals $(1f_{5/2}, 2p_{3/2}, 2p_{1/2}, 1g_{9/2})$. At first, we calculated the energies of the yrast states and the reduced transition strengths of the linking electric quadrupole ($E2$) transitions for varied limitations of occupation numbers to test at which numbers the $B(E2)$ values do not change further and a convergence is achieved. This is in particular important for the midshell isotopes. For example, an increase of the allowed maximum occupation number (upper limit) in the neutron $1g_{9/2}$ orbital from four to six in ^{70}Ge does not change the $B(E2, 2_1^+ \rightarrow 0_1^+)$ value and, thus, the application of an upper limit of four is appropriate. In ^{74}Ge, a change of this number from six to eight changes the $B(E2, 2_1^+ \rightarrow 0_1^+)$ value from 357 to 369 e^2 fm^4, while the further increase to ten neutrons does not cause any further change. At the same time, the allowed minimum occupation numbers (lower limits) in the neutron $2p_{3/2}$ and $1f_{5/2}$ orbitals were set to two. A decrease of these lower limits to zero results in $B(E2, 2_1^+ \rightarrow 0_1^+) = 371$ e^2 fm^4. In the full calculations including all transition strengths, the following limits of occupation numbers were applied to truncate the configuration space and, hence, make the calculations feasible and efficient. Up to four protons were allowed to occupy each of the $1f_{5/2}$ and $2p_{3/2}$ orbitals while up to two could be lifted to each of the $2p_{1/2}$ and $1g_{9/2}$ orbitals. The same holds for the neutrons in ^{64}Ge, while there can be up to six neutrons in the $1f_{5/2}$ orbital in ^{66}Ge. In ^{70}Ge, at least two neutrons are in each of the $1f_{5/2}$ and $2p_{3/2}$ orbitals and up to four can be excited to the $1g_{9/2}$ orbital. The possible occupation numbers of neutrons in the $1g_{9/2}$ orbital are further increased in the heavier isotopes, ranging from two to eight in ^{74}Ge, from six to ten in ^{78}Ge, and from eight to ten in ^{80}Ge. For the calculation of the reduced electric quadrupole transition strengths $B(E2)$, standard effective charges of $e_\pi = 1.5e$ and $e_\nu = 0.5e$ were used, and for the $B(M1)$ strengths effective g factors of $g_s^{\rm eff} = 0.7 g_s^{\rm free}$ were applied.

The full calculations were performed for the lowest 40 states of each spin from $J_i, J_f = 0$ to 10 and each parity. The reduced transition strengths $B(M1)$ were calculated for all transitions from initial to final states with energies $E_f < E_i$ and spins $J_f = J_i, J_i \pm 1$. This resulted in more than 24 000 $M1$ transitions for each parity, which were sorted into 0.1-MeV bins of transition energy $E_\gamma = E_i - E_f$. The average $B(M1)$ value for one energy bin was obtained as the sum of all $B(M1)$ values divided by the number of transitions within this bin. Average $B(E2)$ values were deduced in an analogous way, but include also the $\Delta J = 2$ transitions. $M1$ strength functions were deduced according to

$$f_{M1}(E_\gamma, E_i, J_i, \pi)$$
$$= 16\pi/9(\hbar c)^{-3}\overline{B}(M1, E_i \rightarrow E_f, J_i, \pi)\rho(E_i, J_i, \pi), \quad (1)$$

where the $\overline{B}(M1, E_i \rightarrow E_f, J_i, \pi)$ are averages in considered (E_i, E_f) bins for given J_i and π, and $\rho(E_i, J_i, \pi)$ are the level densities derived from the present calculations. The strength functions $f_{M1}(E_\gamma)$ were obtained by averaging step by step over $E_i, J_i,$ and π.
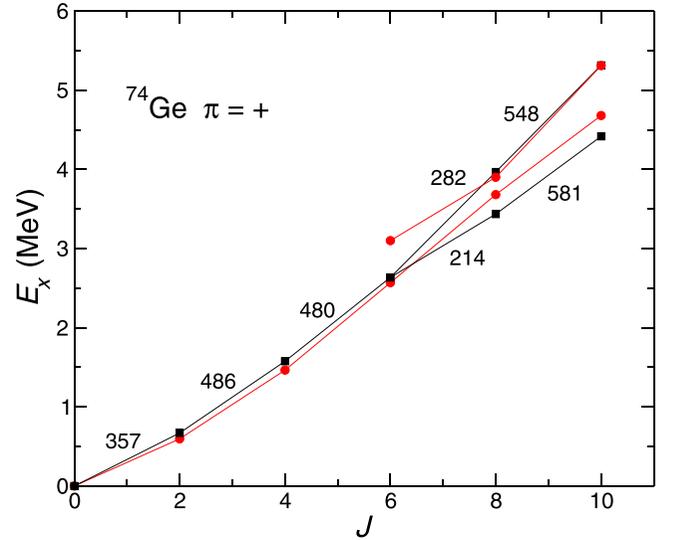

FIG. 1. Experimental (red circles) and calculated (black squares) excitation energies of the yrast states and the states of the first excited band in ^{74}Ge. The lines represent the linking $E2$ transitions with large strengths. The numbers at the lines are calculated $B(E2)$ values in e^2 fm^4. The configuration space allowed up to six neutrons in the $1g_{9/2}$ orbital (see text).

III. RESULTS FOR THE YRAST REGION

To check the reliability of the shell-model calculations, we studied the yrast regions of the Ge isotopes. The calculated energies of the ground-state and first excited bands in ^{74}Ge are compared with the experimental ones [24] in Figs. 1 and 2. They represent the results obtained with the just discussed upper limits of six and eight $1g_{9/2}$ neutrons, respectively. In both cases, the experimental bands are well described by the calculations. A similarly good description of the experimental yrast and yrare bands by the present calculations is achieved
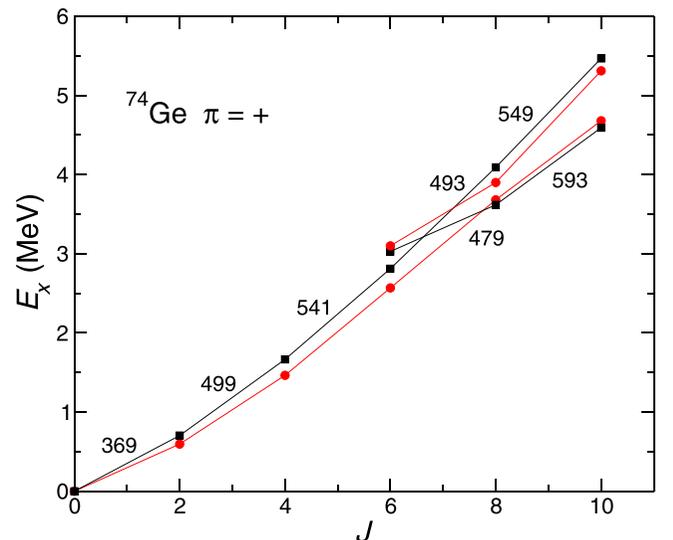

FIG. 2. As Fig. 1, but with a configuration space allowing up to eight neutrons in the $1g_{9/2}$ orbital (see text).

TABLE I. Experimental and calculated reduced $E2$ transition probabilities for the $2_1^+ \to 0_1^+$ transitions in ^{64,66,70,74,78,80}Ge.

	$E(2_1^+)$ (keV)		$B(E2, 2_1^+ \to 0_1^+)$ (e^2 fm^4)		$\Sigma B(E2, 2_n^+ \to 0_1^+)$ (e^2 fm^4)
	EXP[a]	CALC	EXP[a]	CALC	CALC
^{64}Ge$_{32}$	902	883		296	308
^{66}Ge$_{34}$	957	828	190(36)	300	321
^{70}Ge$_{38}$	1040	649	356(7)	336	382
^{74}Ge$_{42}$	596	704	609(7)	369	384
^{78}Ge$_{46}$	619	782	455(79)	320	343
^{80}Ge$_{48}$	659	871	279(55)	233	280

[a]The values for ^{64,66,70,74,78,80}Ge were taken from Refs. [25–30], respectively.

for all other isotopes, which are presented in Figs. 11 and 12 of the Appendix.

In accordance with the experiment, the energies $E(J)$ increase in a regular way, forming quasirotatonal bands. The crossing of the ground-state band with an excited band at $J = 6$ is reproduced. The energy ratios $E(J)/E(2^+)$ deviate substantially from the rotor rule $J(J + 1)$. The calculated ratios $E(4_1^+)/E(2_1^+)$ of 2.44, 2.59, 2.59, 2.38, 2.32, and 2.22 for ^{64,66,70,74,78,80}Ge compare well with experimental ratios of 2.28, 2.27, 2.07, 2.46, 2.54, and 2.64, respectively. They characterize the Ge isotopes as soft nuclei in the transitional region between spherical and deformed shapes, because they are well below the rotor ratio of 3.33. The calculated $B(E2)$ values increase toward high spin up to the crossing region. For ^{74}Ge, the experimental ratio $B(E2, 4_1^+ \to 2_1^+)/B(E2, 2_1^+ \to 0_1^+) = 1.33(8)$ is reproduced by the calculated one of 1.35.

The results for the 2_1^+ states are compared with the experimental values in Table I. The energies of the 2_1^+ states are reproduced within 100 keV, except the high experimental value for ^{70}Ge. The experimental $B(E2, 2_1^+ \to 0_1^+)$ values indicate a maximum of the quadrupole collectivity in the middle of the shell, which is reproduced by the calculations. However, the calculated peak is much shallower than in the experiment. A similar shallow peak is obtained for $J = 4$ and 6 (see Figs. 11 and 12 of the Appendix).

One should be aware that the determination of the quadrupole collectivity from the $B(E2, 2_1^+ \to 0_1^+)$ values only is based on the assumption of a rotational behavior of the yrast states, which is not realized for the soft nuclei under consideration. Instead, the sums of the $B(E2, 0_1^+ \to 2_n^+)$ values of all transitions from the ground state are more appropriate [31,32] and also given in Table I. These sums of all $E2$ transitions into the ground state are however only a little larger and follow the trends of the $B(E2, 2_1^+ \to 0_1^+)$ values. An even more comprehensive indicator of the collectivity may be the consideration of average $B(E2)$ values between all the states considered here. The further discussion of $B(E2)$ values in Sec. IV therefore takes into account these values.

IV. RESULTS FOR THE STRENGTH FUNCTIONS

The average $B(M1)$ and $B(E2)$ values for positive parity states and the $M1$ strength functions including both parities are shown for all considered Ge isotopes in Figs. 3–8. The $N = Z = 32$ nucleus ^{64}Ge shows a fluctuating, but on average flat distribution of the $B(M1)$ strength as a function of E_γ with an even slight decrease toward $E_\gamma = 0$, which is similar to predictions for the $N = Z$ nuclei ^{48}Ca [13] and ^{108}Xe [18]. This seems to point to a more general feature of the low-energy $M1$ strength in $N = Z$ nuclei. It is suggested below that isospin conservation quenches the LEMAR spike. In the $N = Z + 2$ nuclide $^{66}_{32}$Ge$_{34}$, a gradual enhancement of the $M1$ strength toward $E_\gamma = 0$ is seen. The behavior resembles the one in $^{60}_{26}$Fe$_{34}$ [16], but is less pronounced. Both these nuclei are localized near the bottom of the neutron (fpg) shell. For $^{70}_{32}$Ge$_{38}$, the bimodal structure of a LEMAR peak at $E_\gamma = 0$ and a broad SR peak around $E_\gamma = 3$ MeV appears. A similar bimodal distribution is seen in $^{74}_{32}$Ge$_{42}$. This bimodal strength distribution is characteristic for nuclei located well in the open shell, as for example also in $^{64,68}_{26}$Fe$_{38,42}$ [16] and in nuclides with $A > 100$ [18]. The SR peak becomes weak in $^{78}_{32}$Ge$_{46}$ and disappears in $^{80}_{32}$Ge$_{48}$, when approaching the top of the neutron shell. A similar suppression of the SR peak toward the next higher neutron shell was also found in $N \approx 80$ nuclei [18]. The present calculations find a maximum of the SR strength in the middle of the neutron shell that correlates with the clear maximum of the experimental $B(E2, 2_1^+ \to 0_1^+)$ values.
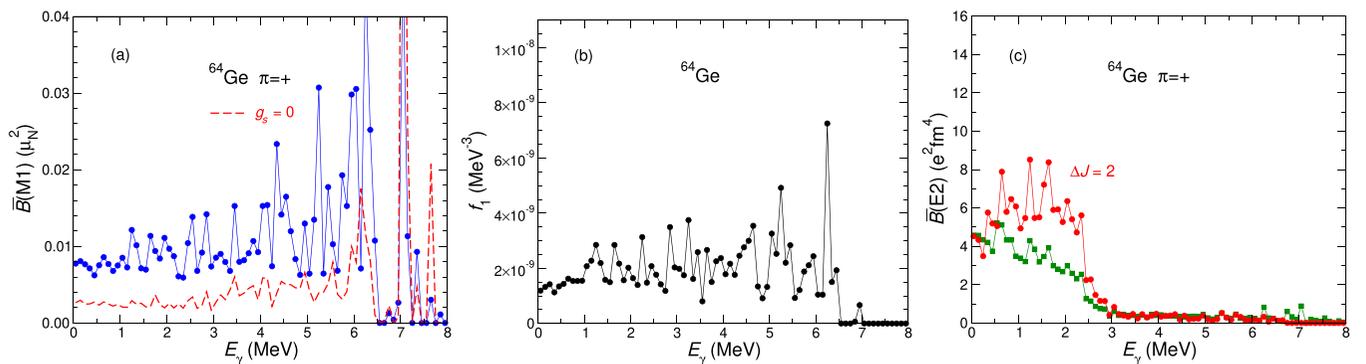

FIG. 3. Results for ^{64}Ge in energy bins of 0.1 MeV. (a) Average reduced $M1$ transition strengths (blue circles) and their orbital contributions ($g_s = 0$) only (red dashed line) for positive-parity states. (b) The $M1$ strength function including both parities. (c) Average reduced $E2$ transition strengths (green squares) and average $B(E2)$ values for stretched transitions with $J_i = J_f + 2$ only (red circles) for positive-parity states.
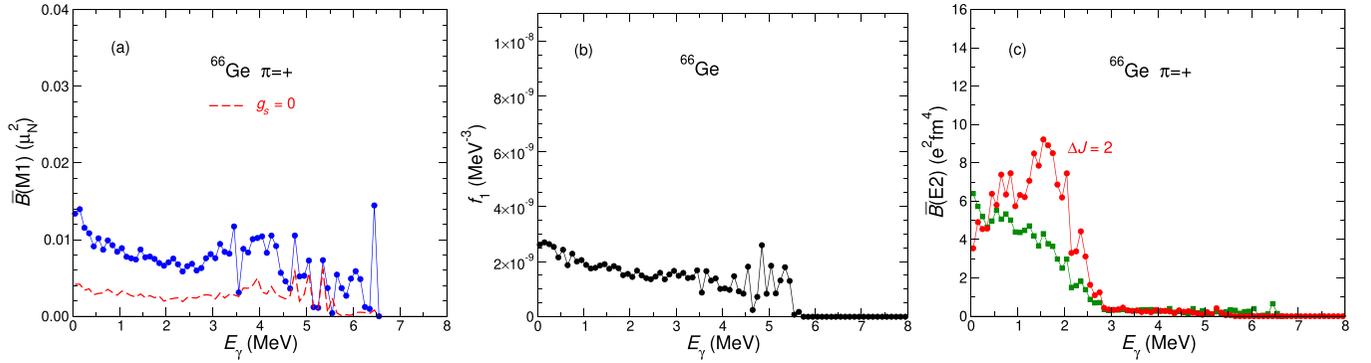
FIG. 4. As Fig. 3, but for ^{66}Ge.

Unlike the experiment, the calculated $B(E2, 2_1^+ \rightarrow 0_1^+)$ values have a very shallow midshell maximum, as was also obtained in the calculations for the Fe isotopes [16].

However, a different behavior is seen for the average $B(E2, J \rightarrow J - 2)$ values shown in panels (c) of Figs. 3–8. Here, a peak around 1 MeV develops toward the middle of the shell (^{70,74}Ge). This peak indicates enhanced collectivity in the $\Delta J = 2$ sequences and clearly correlates with the maximum of the SR strength in the middle of the shell. It can be interpreted as the appearance of damped rotational transitions (see, e.g., Ref. [33]) as a consequence of building up quadrupole collectivity. The calculations include states up to angular momentum 10 $\hbar$ with equal weight. The average transition energy of 1 MeV and the average angular momentum of 5 $\hbar$ correspond to a moment of inertia of about 10 $\hbar^2$/MeV, which is somewhat smaller than the rigid-body value of 14 $\hbar^2$/MeV for $A = 70$. In the same way, from Fig. 4 of Ref. [16] one derives a moment of inertia of 8 $\hbar^2$/MeV for $^{68}_{26}$Fe$_{42}$. In Ref. [6], the increased SR strength of the γ-SF of ^{151,153}Sm could be reproduced by replacing the ground-state moment of inertia by the rigid-body value in the phenomenological expression of Ref. [34], which was developed for the excitation of the SR from the ground state.

We calculated the total $B(M1)$ strengths in certain energy ranges by a numerical integration of the $M1$ strength functions:

$$B(M1)_{\text{tot}} = 9/(16\pi)\,(\hbar c)^3 \sum f_{M1}(E_\gamma)\Delta E_\gamma. \quad (2)$$
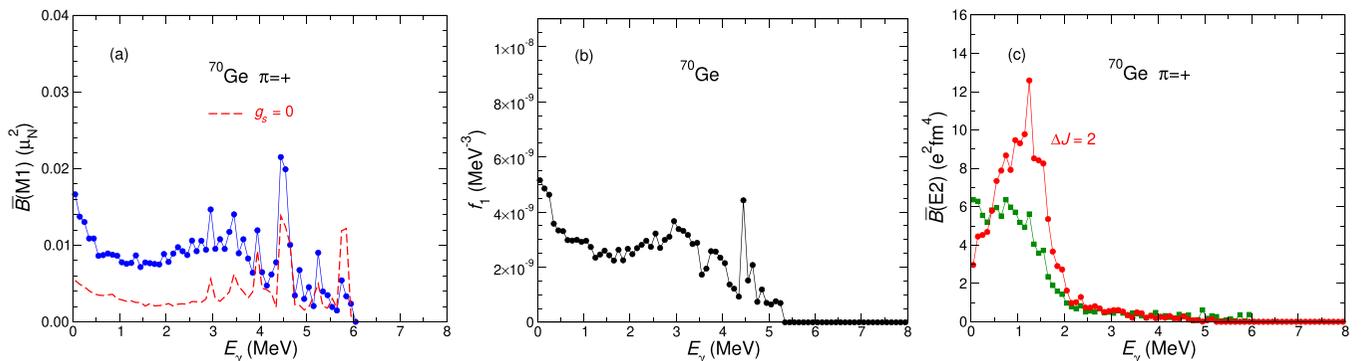
The results for the LEMAR region ($E_\gamma < 2$ MeV), the SR region ($2 \leqslant E_\gamma < 5$ MeV), and their sums are compiled in Table II. As visualized in panels (b) of Figs. 3–8, one also quantitatively observes a shift of strength to the SR region when going into the open shell ($^{70,74}_{32}$Ge$_{38,42}$) and a shift back to the LEMAR region when approaching the $N = 50$ shell closure ($^{78,80}_{32}$Ge$_{46,48}$), while the sum of the two remains roughly constant. Only the $N = Z$ nuclide ^{64}Ge does not fit the systematics for reasons discussed below. In the calculations of Ref. [16], a similar redistribution of the $M1$ strength was found for the isotopes $^{60,64,68}_{26}$Fe$_{34,38,42}$ when moving into the open shell by adding neutrons. However, the integrated strength up to 5 MeV, which is the sum of the LEMAR and SR strength, is about 1 μ_N^2 for the Ge isotopes and about 10 μ_N^2 for the Fe isotopes. The authors of Ref. [11] suggested that the low-energy $M1$ radiation is generated by the reorientation of the valence nucleons on high-j orbitals. This mechanism is particular efficient if protons are holelike and neutrons are particlelike (or vice versa). Then the transverse magnetic moments add up, which generates strong $M1$ radiation. An analogous mechanism generates the "shears bands" manifesting "magnetic rotation" [35]. In the case of the Fe isotopes one has active $1f_{7/2}$ proton holes, which favorably combine with the active $1g_{9/2}$ neutrons. In the case of the Ge isotopes the active $1g_{9/2}$ neutrons combine with the $1f_{5/2}$ protons, which have a small magnetic moment, and $1g_{9/2}$ protons, which have a magnetic moment with the opposite sign. The factor of 10 in the integrated low-energy $M1$ strength reflects the different valence proton configurations of the Fe and Ge isotopes. In


FIG. 5. As Fig. 3, but for ^{70}Ge.
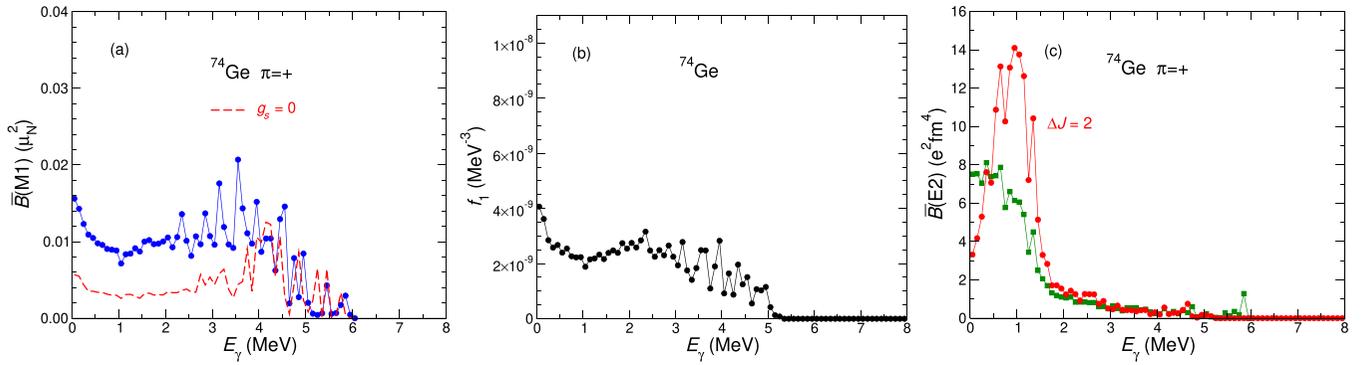
FIG. 6. As Fig. 3, but for ^{74}Ge.

case of the $Z > 50$, $N \geqslant 80$ nuclides the integrated strength up to 4 MeV is $0.5 - 1\mu_N^2$ (see Fig. 3 of Ref. [18]). The small number is expected because active protons and neutrons are particlelike and do not occupy the high-j orbitals.

Also shown in Table II are the integrated $B(E2)$ strengths up to $E_\gamma = 5$ MeV, which were determined analogously to the integrated $B(M1)$ strengths. The values are maximal at the midshell nuclei ^{70,74}Ge in accordance with the SR strengths, which proves the correlation of SR strength and collectivity.

The excitation of the SR from the ground state, which appears as a bunch of 1^+ states around 3 MeV, has been extensively studied and reviewed in Ref. [15]. Therein, the SR is considered as being dominated by exciting the orbital angular momentum of the protons. In contrast, our calculations for the Ge isotopes show a reduction of the low-energy strength by a factor of about 2 when the spin part of the magnetic dipole operator is set equal to zero, which is illustrated in panels (a) of Figs. 3–8. An equal reduction appeared in our earlier calculations for the Mo and Fe isotopes as displayed in Figs. 9 and 10. The strong dependence of the $M1$ strength on the spin part indicates that the reorientation of high-j orbitals such as $1g_{9/2}$ and $1h_{11/2}$ must play a central role in generating the strong $M1$ radiation (see Ref. [16]). In the calculations for ^{130}Te in Ref. [18], the SR peak is similarly quenched when the spin part of the $M1$ operator is set equal to zero whereas the LEMAR spike remains unchanged [see Figs. 2(c) and 2(d) therein].

The SR strength in the medium and heavy nuclei has been found proportional to the square of the quadrupole deformation, which is maximal in the middle of the open shell [15]. As discussed in Ref. [6], the strength of the SR in the γ-SF seems to be related to the nuclear ground-state deformation in a similar way, though being a factor of 3 larger. The calculations in Ref. [18] show the buildup of a SR around 4 MeV when moving into the open shell by adding neutrons in the case of the Te isotopes and when adding protons in the case of the $N = 80$ isotones, where the SR strength increases with the $B(E2, 2_1^+ \rightarrow 0_1^+)$ values (compare Figs. 1 and 3 in Ref. [18]) and the experimental values for the studied nuclides given in Ref. [36]). The same correlation between the increase of experimental $B(E2, 2_1^+ \rightarrow 0_1^+)$ and the increase of the SR strength was found for the Fe isotopes in the calculations in Ref. [16].

The integrated strengths up to a transition energy of 5 MeV in Table II are about $1 \mu_N^2$. They are much larger than the sums of the strengths of transitions from 1^+ states down to the ground state, which are also given in Table II. As seen in Table II of Ref. [16], the integrated strengths up to a transition energy of 5 MeV in ^{60,64,68}Fe are about $10 \mu_N^2$ to be compared with 0.33, 0.55, and $0.58 \mu_N^2$ for the respective sums of all transitions from 1^+ states down to the ground state. In Ref. [7], the experimental integrated $M1$ strengths up to 5 MeV for transitions in the quasicontinuum of ^{147,149,151,153}Sm were found to be about $8 \mu_N^2$, which has to be compared with summed strengths of 0.16, 0.32, 0.80, and $0.81 \mu_N^2$ from 1^+
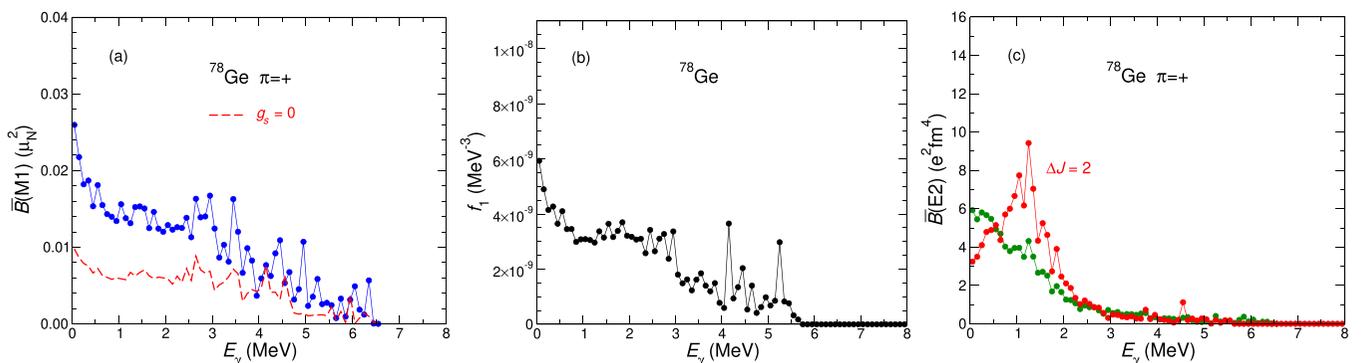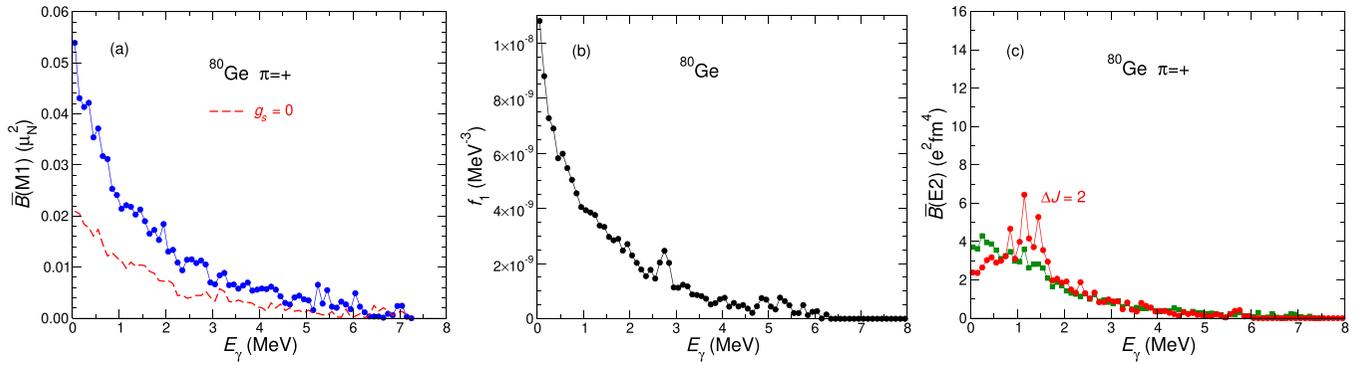

FIG. 7. As Fig. 3, but for ^{78}Ge.

FIG. 8. As Fig. 3, but for ^{80}Ge. Note the different vertical scale in panel (a) compared with the corresponding graphs for the other isotopes.

states to the ground states of ^{148,150,152,154}Sm, respectively [34]. In Ref. [16], the enhancement was attributed to the quenching of the pair correlations with increasing excitation energy, i.e., the thermal quenching of pairing.

According to the collective model of Ref. [34], the $M1$ strength of the SR on the ground state scales $\propto A\delta^2$, where δ is the deformation parameter and A the mass number. The sums $\sum B(M1, 1^+ \rightarrow 0_1^+)$ of transition down to the ground states of the Ge, Fe, Te, and Sm isotopes roughly follow the scaling (see Table II and Refs. [7,16,18]). The simple collective behavior seems to be caused by the pair correlations. The integrated $M1$ strengths for the transitions in the quasicontinuum do not obey it. Once the pair correlations are quenched, the bimodal LEMAR-SR structure appears in the strength function, the total strength of which depends strongly on the individual magnetic properties of the valence nucleons. This is in analogy to the moments of inertia. At low spin, when the the pair correlations are strong, the moments of inertia behave in a systematic manner, being $\propto A^{5/3}\delta^2$. At high spin, when the Coriolis force overcomes the pair correlation, the individuality of the valence nucleons comes to light.

The experimental summed strengths for the transitions from 1^+ states to the ground state given in Table II are smaller than the calculated ones. However, the experimental values represent only a lower limit. In the calculations, a large number of weak transitions contributes to the summed strengths, whereas experiments such as the ones in Ref. [37] detect only the strongest transitions. It has been demonstrated that a large number of weak transitions, which are hidden in a quasicontinuum, may substantially enlarge the $M1$ strength function, as seen for example in Ref. [38].

The $M1$ operator has approximately isospin $T = 1$ character. In $N = Z$ nuclei the low-lying states have $T = 0$. The $T = 1$ states lie substantially higher. In case of ^{64}Ge, the experimental energy of the lowest $T = 1$ state is 6.2 MeV. Thus, the sum $\sum B(M1, 1^+ \rightarrow 0_1^+) = 0.001 \mu_N^2$ in Table II includes only transitions between $T = 0$ states, which are isospin forbidden. The very small value for ^{64}Ge reflects that isospin conservation nearly quenches $M1$ transitions between the $T = 0$ states. For $N = Z + 2$ nuclei the low-lying states have $T = 1$. Transitions between $T = 1$ states are allowed, which results in $\sum B(M1, 1^+ \rightarrow 0_1^+) = 0.25\mu_N^2$ for ^{66}Ge. One expects that the same mechanism works for higher excitation energies. Transitions between the $T = 0$ states are nearly forbidden. The $T = 1$ states lie on the average substantially
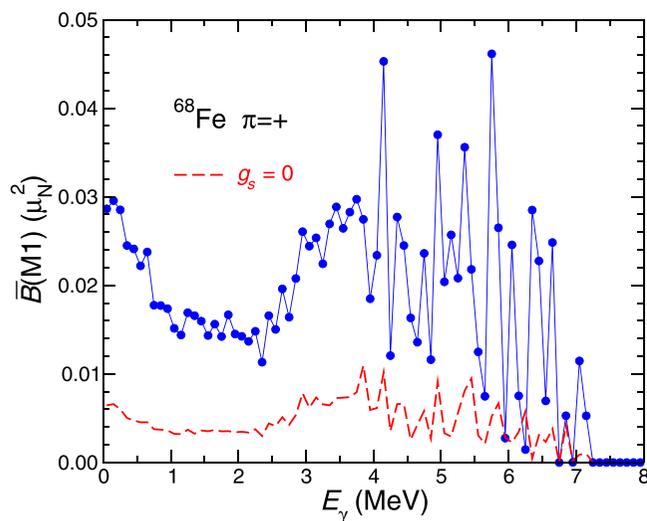

FIG. 9. As Fig. 3(a), but for ^{68}Fe. The corresponding shell-model calculations are described in Ref. [16].
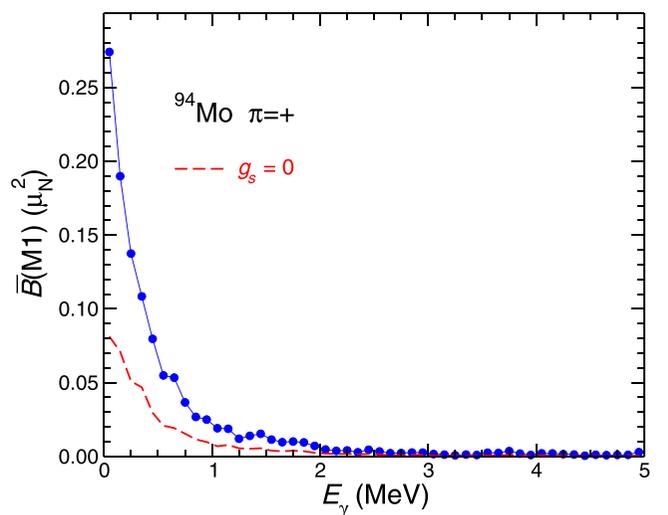

FIG. 10. As Fig. 3(a), but for ^{94}Mo. The corresponding shell-model calculations are described in Ref. [11].

TABLE II. Summed $B(M1)$ strengths in ranges of transition energy (LEMAR, $E_\gamma < 2$ MeV; scissors, 2 MeV $\leqslant E_\gamma < 5$ MeV; $\sum$, the sum of the two), summed $B(E2)$ strengths for $E_\gamma < 5$ MeV, and summed strengths of all discrete transitions from 1^+ states to the ground states in ^{64,66,70,74,78,80}Ge.

	$B(M1)_{\text{tot}}$[a] (μ_N^2)			$B(E2)_{\text{tot}}$[b] $(e^2 \text{ fm}^4)$	$\sum B(M1, 1^+ \to 0_1^+)$[c] (μ_N^2)	
	LEMAR	SR	$\sum$		EXP[d]	CALC
^{64}Ge$_{32}$	0.30	0.54	0.84	155		0.001
^{66}Ge$_{34}$	0.35	0.35	0.70	185		0.25
^{70}Ge$_{38}$	0.54	0.62	1.16	219	0.04(1)	0.49
^{74}Ge$_{42}$	0.44	0.50	0.94	241	0.30(3)	0.57
^{78}Ge$_{46}$	0.63	0.49	1.12	181		0.48
^{80}Ge$_{48}$	0.84	0.28	1.12	123		0.31

[a]Integrated $M1$ strength calculated according to Eq. (2).

[b]Integrated $E2$ strength calculated for positive-parity states in analogy to Eqs. (1) and (2).

[c]Summed $M1$ strength of transitions from the 1^+ states below 5 MeV to the ground state.

[d]Value taken from Ref. [37].

above the $T = 0$ states that are connected by the $M1$ operator, which prevents transition energies close to zero. For $N > Z$ nuclides, the transitions between the states with the same isospin $T > 0$ are allowed and the LEMAR spike appears. The author of Ref. [18] suggested an alternative explanation: $N = Z$ nuclei have a particular large deformation that moves $M1$ strength from the LEMAR spike to the SR, which results in a flat distribution. At variance, the N dependences of the $E2$ strength in Figs. 3–8 and Table II indicate little $E2$ collectivity for ^{64}Ge.

V. SUMMARY

Shell-model calculations were performed for the series of germanium isotopes with neutron numbers from $N = 32$ to 48. Average $B(M1)$ and $B(E2)$ strengths were determined from a large number of transitions linking states of spins from 0 to 10. The average $B(M1)$ strengths and the associated $M1$ strength functions are strongly enhanced near zero transition energy, which is the LEMAR spike observed before. The LEMAR spike develops with increasing neutron number and is strongest at $N = 80$. It is suppressed at $N = Z$, which is attributed to isospin conservation. In the midshell nuclei, a bump around 3.5 MeV appears, which is interpreted as the scissors resonance. The strength of the SR correlates with the quadrupole collectivity, as reflected by the experimental $B(E2, 2_1^+ \to 0^+)_1$ values and the integrated average $E2$ strength of quasicontinuum transitions. The sum of the LEMAR and SR strengths depends only weakly on the neutron number. These characteristics are consistent with those found for the series of iron isotopes and with the experimental observation of LEMAR and SR strengths in samarium isotopes as well. They exhibit the important role of high-j orbitals, such as $1g_{9/2}$ and $1h_{11/2}$, for the evolution of the low-lying modes. Spin and orbital contributions to the $M1$ strength appear nearly equal at low energy in most isotopes, while there are stronger orbital contributions above 4 MeV of transition energy in the midshell isotopes ^{70,74}Ge. The present systematic analysis of low-lying $M1$ strength in a relatively long isotopic series demonstrates that the correlated appearance of the two $M1$ modes is a phenomenon that occurs across various mass regions.

ACKNOWLEDGMENTS

APPENDIX: YRAST PROPERTIES OF THE REMAINING ISOTOPES

Figures 11 and 12 show excitation energies versus spin of experimental and calculated yrast states.
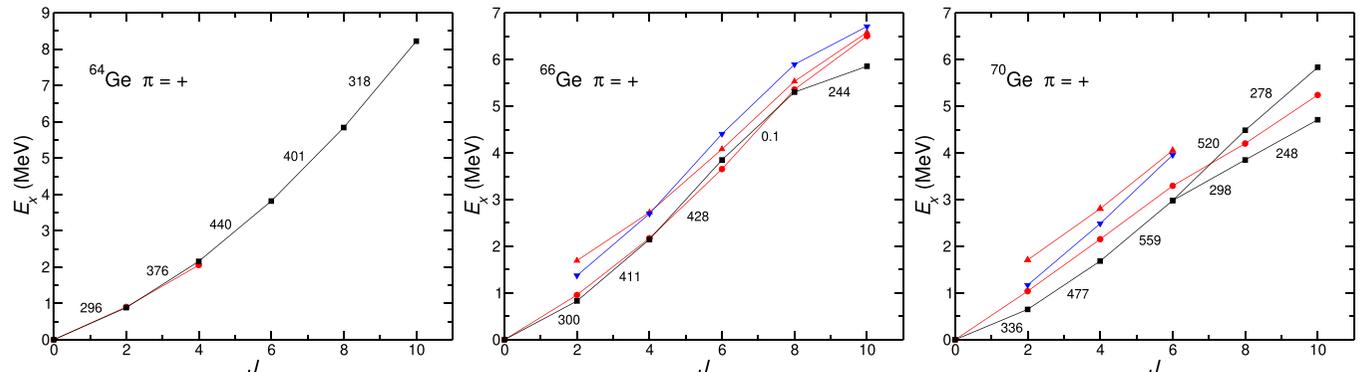

FIG. 11. Excitation energies vs spin of experimental (red circles) and calculated (black squares) yrast states in ^{64,66,70}Ge, and of experimental (red triangles up) and calculated (blue triangles down) states built on the second 2^+ states in ^{66,70}Ge. The lines represent the linking $E2$ transitions. The numbers at the lines are calculated $B(E2)$ values in e^2 fm^4. The experimental data were taken from Refs. [39–41], respectively.
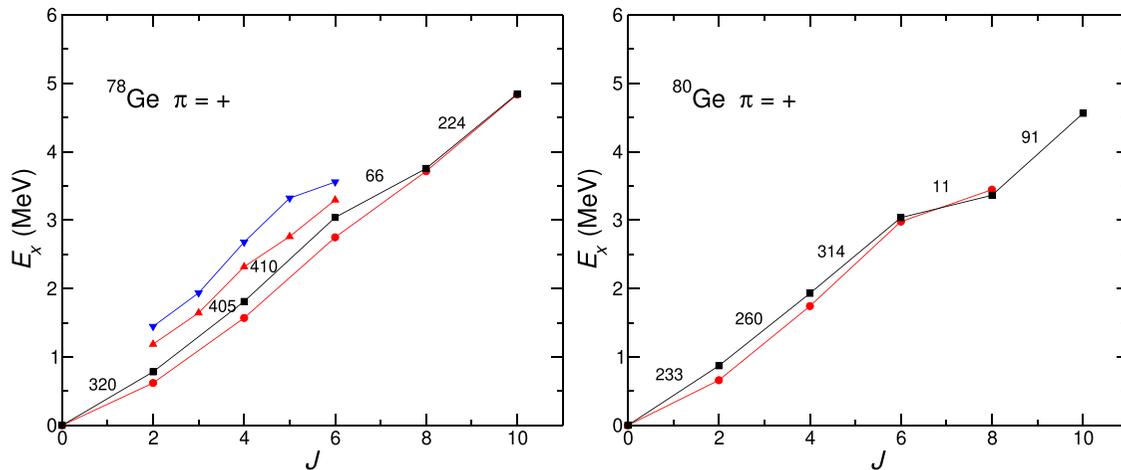
FIG. 12. Excitation energies vs spin of experimental (red circles) and calculated (black squares) yrast states in ^{78,80}Ge, and of experimental (red triangles up) and calculated (blue triangles down) states built on the second 2^+ state in ^{78}Ge. The lines represent the linking $E2$ transitions. The numbers at the lines are calculated $B(E2)$ values in e^2 fm^4. The experimental data were taken from Refs. [42,43], respectively.

[1] M. Arnould, S. Goriely, and K. Takahashi, Phys. Rep. **450**, 97 (2007).

[2] F. Käppeler, R. Gallino, S. Bisterzo, and W. Aoki, Rev. Mod. Phys. **83**, 157 (2011).

[3] A. Voinov, E. Algin, U. Agvaanluvsan, T. Belgya, R. Chankova, M. Guttormsen, G. E. Mitchell, J. Rekstad, A. Schiller, and S. Siem, Phys. Rev. Lett. **93**, 142504 (2004).

[4] M. Guttormsen, R. Chankova, U. Agvaanluvsan, E. Algin, L. A. Bernstein, F. Ingebretsen, T. Lonnroth, S. Messelt, G. E. Mitchell, J. Rekstad, A. Schiller, S. Siem, A. C. Sunde, A. Voinov, and S. Odegard, Phys. Rev. C **71**, 044307 (2005).

[5] A. C. Larsen, I. E. Ruud, A. Burger, S. Goriely, M. Guttormsen, A. Görgen, T. W. Hagen, S. Harissopulos, H. T. Nyhus, T. Renstrøm, A. Schiller, S. Siem, G. M. Tveten, A. Voinov, and M. Wiedeking, Phys. Rev. C **87**, 014319 (2013).

[6] A. Simon, M. Guttormsen, A. C. Larsen, C. W. Beausang, P. Humby, J. T. Harke, R. J. Casperson, R. O. Hughes, T. J. Ross, J. M. Allmond, R. Chyzh, M. Dag, J. Koglin, E. McCleskey, M. McCleskey, S. Ota, and A. Saastamoinen, Phys. Rev. C **93**, 034303 (2016).

[7] F. Naqvi, A. Simon, M. Guttormsen, R. Schwengner, S. Frauendorf, C. S. Reingold, J. T. Harke, N. Cooper, R. O. Hughes, S. Ota, and A. Saastamoinen, Phys. Rev. C **99**, 054331 (2019).

[8] A. Spyrou, S. N. Liddick, A. C. Larsen, M. Guttormsen, K. Cooper, A. C. Dombos, D. J. Morrissey, F. Naqvi, G. Perdikakis, S. J. Quinn, T. Renstrøm, J. A. Rodriguez, A. Simon, C. S. Sumithrarachchi, and R. G. T. Zegers, Phys. Rev. Lett. **113**, 232502 (2014).

[9] A. C. Larsen, N. Blasi, A. Bracco, F. Camera, T. K. Eriksen, A. Görgen, M. Guttormsen, T. W. Hagen, S. Leoni, B. Million, H. T. Nyhus, T. Renstrøm, S. J. Rose, I. E. Ruud, S. Siem, T. Tornyi, G. M. Tveten, A. V. Voinov, and M. Wiedeking, Phys. Rev. Lett. **111**, 242504 (2013).

[10] A. Voinov, S. M. Grimes, C. R. Brune, M. Guttormsen, A. C. Larsen, T. N. Massey, A. Schiller, and S. Siem, Phys. Rev. C **81**, 024319 (2010).

[11] R. Schwengner, S. Frauendorf, and A. C. Larsen, Phys. Rev. Lett. **111**, 232504 (2013).

[12] B. A. Brown and A. C. Larsen, Phys. Rev. Lett. **113**, 252502 (2014).

[13] K. Sieja, EPJ Web Conf. **146**, 05004 (2017).

[14] K. Sieja, Phys. Rev. Lett. **119**, 052502 (2017).

[15] K. Heyde, P. von Neumann-Cosel, and A. Richter, Rev. Mod. Phys. **82**, 2365 (2010).

[16] R. Schwengner, S. Frauendorf, and B. A. Brown, Phys. Rev. Lett. **118**, 092502 (2017).

[17] S. Karampagia, B. A. Brown, and V. Zelevinsky, Phys. Rev. C **95**, 024322 (2017).

[18] K. Sieja, Phys. Rev. C **98**, 064312 (2018).

[19] J. E. Midtbø, A. C. Larsen, T. Renstrøm, F. L. Bello Garrote, and E. Lima, Phys. Rev. C **98**, 064321 (2018).

[20] M. Honma, T. Otsuka, T. Mizusaki, and M. Hjorth-Jensen, Phys. Rev. C **80**, 064323 (2009).

[21] B. A. Brown and A. F. Lisetskiy (unpublished).

[22] A. F. Lisetskiy, B. A. Brown, M. Horoi, and H. Grawe, Phys. Rev. C **70**, 044314 (2004).

[23] B. A. Brown and W. D. M. Rae, Nucl. Data Sheets **120**, 115 (2014).

[24] J. J. Sun, Z. Shi, X. Q. Li, H. Hua, C. Xu, Q. B. Chen, S. Q. Zhang, C. Y. Song, J. Meng, X. G. Wu, S. P. Hu, H. Q. Zhang, W. Y. Liang, F. R. Xu, Z. H. Li, G. S. Li, C. Y. He, Y. Zheng, Y. L. Ye, D. X. Jiang et al., Phys. Lett. B **734**, 308 (2014).

[25] B. Singh, Nucl. Data Sheets **108**, 197 (2007).

[26] E. Browne and J. K. Tuli, Nucl. Data Sheets **111**, 1093 (2010).

[27] G. Gürdal and E. A. Mccutchan, Nucl. Data Sheets **136**, 1 (2016).

[28] B. Singh and A. R. Farhan, Nucl. Data Sheets **107**, 1923 (2006).

[29] A. R. Farhan and B. Singh, Nucl. Data Sheets **110**, 1917 (2009).

[30] B. Singh, Nucl. Data Sheets **105**, 223 (2005).

[31] K. Kumar, Phys. Rev. Lett. **28**, 249 (1972).

[32] A. Poves, F. Nowacki, and Y. Alhassid, Phys. Rev. C **101**, 054307 (2020).

[33] M. Matsuo, T. Dossing, E. Vigezzi, R. A. Broglia, and K. Yoshida, Nucl. Phys. A **617**, 1 (1997).

[34] J. Enders, P. von Neumann-Cosel, C. Rangacharyulu, and A. Richter, Phys. Rev. C **71**, 014306 (2005).

[35] S. Frauendorf, Rev. Mod. Phys. **73**, 463 (2001).

[36] S. Raman, C. W. Nestor, Jr., and P. Tikkanen, At. Data Nucl. Data Tables **78**, 1 (2001).

[37] A. Jung, S. Lindenstruth, H. Schacht, B. Starck, R. Stock, C. Wesselborg, R. D. Heil, U. Kneissl, J. Margraf, H. H. Pitz, and F. Steiper, Nucl. Phys. A **584**, 103 (1995).

[38] R. Massarczyk, G. Rusev, R. Schwengner, F. Dönau, C. Bhatia, M. E. Gooden, J. H. Kelley, A. P. Tonchev, and W. Tornow, Phys. Rev. C **90**, 054310 (2014).

[39] E. Farnea, G. de Angelis, A. Gadea, P. G. Bizzeti, A. Dewald, J. Eberth, A. Algora, M. Axiotis, D. Bazzacco, A. M. Bizzeti-Sona *et al.*, Phys. Lett. B **551**, 56 (2003).

[40] E. A. Stefanova, I. Stefanescu, G. de Angelis, D. Curien, J. Eberth, E. Farnea, A. Gadea, G. Gersch, A. Jungclaus, K. P. Lieb, T. Martinez, R. Schwengner, T. Steinhardt, O. Thelen, D. Weisshaar, and R. Wyss, Phys. Rev. C **67**, 054319 (2003).

[41] B. Mukherjee, S. Muralithar, G. Mukherjee, R. P. Singh, R. Kumar, J. J. Das, P. Sugathan, N. Madhavan, P. V. M. Rao, A. K. Sinha, A. K. Pande, L. Chaturvedi, S. C. Pancholi, and R. K. Bhowmik, Acta Phys. Hung. N. S. **11**, 189 (2000); **13**, 253(E) (2001).

[42] A. M. Forney, W. B. Walters, C. J. Chiara, R. V. F. Janssens, A. D. Ayangeakaa, J. Sethi, J. Harker, M. Alcorta, M. P. Carpenter, G. Gürdal, C. R. Hoffman, B. P. Kay, F. G. Kondev, T. Lauritsen, C. J. Lister, E. A. McCutchan, A. M. Rogers, D. Seweryniak, I. Stefanescu, and S. Zhu, Phys. Rev. Lett. **120**, 212501 (2018).

[43] Zs. Podolyak, S. Mohammadi, G. de Angelis, Y. H. Zhang, M. Axiotis, D. Bazzacco, P. G. Bizetti, F. Brandolini, R. Broda, D. Bucurescu, E. Farnea *et al.*, Int. J. Mod. Phys. **13**, 123 (2004).